ceramics

MDPI

Article

Computational Investigation of the Influencing Parameters on the Solidification of Thermoplastic Beryllium Oxide Slurry in a Cylindrical Shell

Zamira Sattinova [1,*], Bakytzhan Assilbekov [2], Tassybek Bekenov [1,*] and Gaukhar Ramazanova [3]

[1] Faculty of Transport and Energy, L.N. Gumilyov Eurasian National University, Astana 010008, Kazakhstan
[2] Laboratory of Computational Modeling and Information Technologies, Satbayev University, Almaty 050013, Kazakhstan; assilbekov.b@gmail.com
[3] Energy Modeling Laboratory, Satbayev University, Almaty 050013, Kazakhstan; gaukhar.ri@gmail.com
* Correspondence: sattinova.kz@gmail.com (Z.S.); tas-bek@mail.ru (T.B.); Tel.: +7-71-7270-9500 (Z.S.)

Abstract: This article presents a computational study of the influencing parameters on the solidification of the thermoplastic beryllium oxide slurry in an annular forming cavity. The main purpose of this paper is to study the effect of cooling and casting conditions on the solidification of the BeO suspension by considering the temperature-dependent rheological and physical properties. The results of calculations of the Bingham–Papanastasiou rheological model with experimental data in the intervals of phase transitions with different casting rates of beryllium ceramics have been validated. The use of the regularization parameter made it possible to approximate the flow of the slurry at all levels of its shear rates as highly viscous, followed by a continuous transition to a solid state. The speed of heat removal from the molding during the solidification period is determined by the speed of movement of the slurry and the temperature field on which the width of the transition region depends. The process of solidification of the slurry mass has been evaluated by changing its heat flow distribution and density along the length of the concentric channel. The obtained model calculation results make it possible to control the casting process and eventually realize a uniform structure of castings.

Keywords: beryllium oxide; continuous casting; solidification; parametric study; CFD model

Citation: Sattinova, Z.; Assilbekov, B.; Bekenov, T.; Ramazanova, G. Computational Investigation of the Influencing Parameters on the Solidification of Thermoplastic Beryllium Oxide Slurry in a Cylindrical Shell. *Ceramics* **2024**, *7*, 906–925. https://doi.org/10.3390/ceramics7030059

Academic Editor: Francesco Scotognella

Received: 9 May 2024
Revised: 24 June 2024
Accepted: 27 June 2024
Published: 1 July 2024

1. Introduction

In recent decades, products derived from thermoplastic beryllium oxide (BeO) have been widely used in various industries, primarily as a heat-dissipating and electrical resistance material for equipment operating under high temperatures [1,2]. At the same time, ceramics produced on the basis of BeO are excellent for implementation in the field of special metallurgy, nuclear equipment, electronics, and the space industry due to their high isolation, low dielectric permeability, high heat conductivity, and excellent temperature-controlled properties [3,4]. Using the hot casting method, ceramic articles of a predetermined shape and size with an adjustable density can be obtained in an industrial casting facility. However, the high thermal conductivity of BeO during casting in the temperature range of 40–55 °C causes difficulty in controlling the structure formation [5]. The solidification mechanism and the mechanical behavior of the casting mass during casting and the rheological and thermophysical properties of thermoplastic BeO slurry following ultrasound exposure have not been well studied. Nevertheless, experimental data allow us to conclude that the effect of ultrasonic vibrations on the slurry mass leads to a change in structure, an increase in technological properties, a decrease in heterogeneity, and a change in rheological properties. In the course of our experiments, the effect of ultrasonic treatment and its duration on the change in viscosity and ultimate shear stress of the slurry depending on temperature (55–75 °C) and the mass fraction of the binder (10–11.7%) have

been studied [6]. At the same time, changes in these properties before and after ultrasound exposure have been analyzed, as well as the nature of the flow in the system under study. The experience of operating the unit with ultrasonic impact has shown that the casting capacity of the slurry increases by an average of 15%, and at the same time, the viscosity decreases by more than half [7]. The experimental study of physicochemical properties and phase change with simultaneous consideration of all factors affecting the quality of products in the process of continuous casting is labor-intensive. Therefore, an effective way to control the physical processes occurring in the formation of articles with predetermined properties and shapes is to simulate the process and determine its basic characteristics.

An analysis of most experimental works devoted to the study of the influence of the main parameters of casting shows that the nature of the process of filling the forming cavity with a slurry depends on the combined influence of speed, force, and temperature factors. These factors depend on a number of process parameters. In particular, the value of the volumetric filling rate and the duration of cooling of the casting at all stages depend on its geometry, the thermophysical properties of the slurry, etc. [4,8,9]. It was experimentally established [10] that a sharp increase in temperature leads to the likelihood of internal shells forming due to an increase in the shrinkage of the slurry [11]. The high thermal conductivity of BeO has a significant influence on the increase in the volume of the liquid phase and the rheology of the thermoplastic slurry during preparation and casting [12]. The thermal conductivity of BeO with a relative density of 99% is 220–230 W/(m·°C) at a temperature of 100 °C [2]. However, with an increase in shrinkage looseness to 5–10% and zonal liquation, the thermal conductivity of ceramics at low temperatures decreases by 10–13% [5]. As the temperature increases, the thermal conductivity decreases and reaches a value of 15.4 W/(m·°C) [12]. Therefore, when considering the object under study, such factors as the dependence of thermophysical properties on temperature, the phase change in liquid suspensions into a solid state, the heat of crystallization, and a sharp change in the temperature boundary conditions on the cooling circuits should be considered. As mentioned in other studies on MIM technology, the increase in the volume of the liquid phase to give the necessary casting properties to the slurry does not allow the required effect to be achieved, since during firing, an "additional" amount of binder leads to the appearance of structural defects and deformations of articles [6]. When forming articles in a forming cavity, control over the cooling of the slurry mass is of great importance, since the process of hardening inside the mass depends on the temperature distribution [13]. Also, the change in the temperature field during cooling depends on the heat release in the phase transition region and the determination of boundary conditions. Experimentally, the established liquidus and solidus temperatures of the BeO slurry make it possible to identify the nature of the phase distribution at different stages of crystallization and to calculate the rate of solid phase separation necessary for studying thermal processes and analyzing the formation of shrinkage defects [8,11].

The main purpose of this paper is to study the effect of cooling and casting conditions on the solidification of thermoplastic beryllium oxide slurry by considering the temperature-dependent rheological and physical properties. According to the experimental data [5], the Bingham–Papanastasiou model with a regularization parameter is used to validate experimental curves and describe the behavior of the thermoplastic slurry with temperature-dependent yield stress and plastic viscosity when treated with ultra-sonic exposure [14–16].

2. Materials

2.1. Characteristics of Beryllium Oxide Powder and Thermoplastic Slurry

Thermoplastic slurry based on BeO powder and organic binder is considered in this simulation. It is a highly viscous suspension in which the solid phase is BeO powder and liquid phase is organic binder. Beryllium oxide powder obtained by standard technology at serial production of JSC at the Ulba metallurgical plant, located in Kazakhstan, is used to prepare the slurry [8]. The organic binder contains paraffin (82%), beeswax (15%), and oleic acid (3%) [6]. The experimental data of BeO powder [17] and organic binder are

given, since the volumetric phase composition and its relationship with the rheological properties of the slurry is the main technological characteristic of the casting system (Tables 1 and 2). Grain size of BeO powder varies from 1.4–4 μm to 50–70 μm depending on its production technology.

Table 1. Characteristics of beryllium oxide powder.

Powder, Grade	Particle Size, μm	t_m, °C	Apparent Density, g/sm^3	Bulk Density, g/sm^3
BeO, H1	1.4–4.2	2570 ± 30	2.30	0.72

Table 2. Composition and properties of organic binder.

Component	Chemical Structure	t_m, °C	Density, g/sm^3		
			20 °C	70 °C	80 °C
Paraffin B2	$C_{18}H_{38}$	52–56	0.918	0.784	0.781
Oleic Acid	$C_{17}H_{33}COOH$	16	0.937	0.886	0.888
Beeswax	$C_3(CH_2)_7CH$	61–63	0.942	0.835	0.827

Composition and properties of casting system are characterized by certain ratio of concentration of powder of beryllium oxide (solid phase C_v), organic binder (liquid phase C_w), critical concentration of solid phase in system C_{vcrit}, fractions of kinetically free C_{Kfree}, and kinetically bound C_{Kbound} liquid (Table 3). The critical concentration of C_{vcrit} is considered an important criterion that objectively characterizes the state of the slurry in determining its properties and structure [8,12].

Table 3. Volume/phase ratios of the thermoplastic BeO slurry.

	Mass Fraction of the Binder w, %	C_v	C_{vcrit}	$\frac{C_v}{C_{vcrit}}$	C_w	C_{Kbound}
BeO	11.7	0.657	0.723	0.908	0.092	0.251
	10.7	0.679	0.728	0.932	0.068	0.253
	10.0	0.695	0.734	0.946	0.054	0.251

For the BeO slurry, the technologically acceptable concentration of the solid phase is 80–85% [8].

C_{Kbound} is a kinetically bound liquid consisting of C_{wm} (mechanically trapped) and C_{wf} (physically and chemically bound) liquids [16]. The proportion of mechanically bound fluid (pinched between particles with their boundary solvate shells) characterizes the degree of stabilization of the solid phase [18]. The physically bound liquid is removed from the preform at a temperature above 100 °C. The mechanically entrapped liquid fills the void between the particles with their boundary solvate shells, and part of the chemically bound liquid passes into the solid phase, creating a solvated shell around the particles of the dispersed phase of the thermoplastic slurry. The structure of these shells is characterized by an oriented structure of molecules, especially in the first few layers immediately adjacent to the surface of the solid particle (Figure 1).

High-quality molding of ceramic articles with uniform properties is achieved by increasing the flow rate of the slurry due to intensive ultrasonic processing with a frequency of 16–18 kHz [12]. The increase in flow of the suspension is accompanied by a decrease in the thickness of the solvated shell and an increase in the amount of free bond (Figure 1). The amount of kinetically bound ligament in the slurry with different volume concentration is $C_{wf} = 0.117$. Improving the flow rate of the slurry leads to a decrease in viscosity, which is one of the main indicators of the relationship between the concentration of the slurry and its rheological properties [8,19].

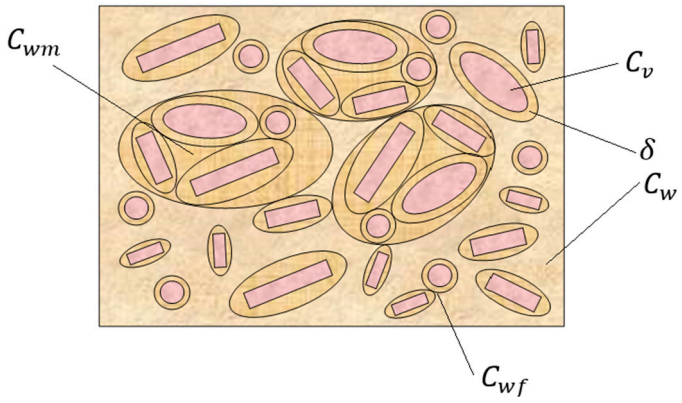

Figure 1. Schematic diagram of thermoplastic BeO slurry structure: C_{wm}—mechanically trapped liquids; C_{wf}—physically and chemically bound liquids; C_v—solids concentration; C_w—liquid phase concentration; δ—solvation shell.

Rheological properties of the slurry, such as yield strength, plastic viscosity, and shear rate in the investigated temperature range of 80 ÷ 40 °C at different durations of ultrasonic treatment, were determined experimentally using a rotational viscometer RV-US (Figure 2b) [6,8].

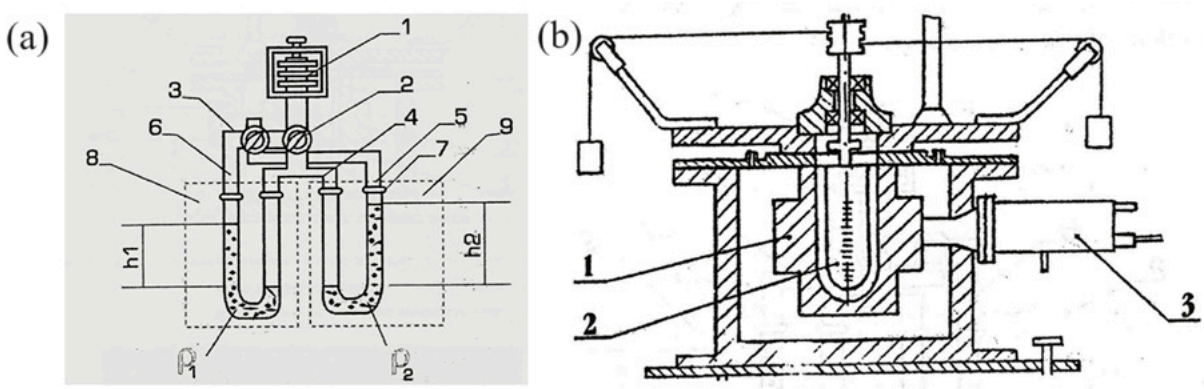

Figure 2. Schematic diagrams of the installation for (**a**) determining the density of binder and (**b**) the rheological properties of the slurry on the RV-US. (**a**) 1—bellows; 2, 3—three-way valves; 4, 5—connecting tubes; 6, 7—U-shaped pressure gauges; 8, 9—thermostats. (**b**) 1—outer cylinder—long-transverse waveguide; 2—internal cylinder; 3—magnetostrictive converter.

Curves $\mu(T)$, $\tau(T)$, taken at the given setups (Figure 3) in the investigated temperature range under different experimental conditions, are approximated by empirical Formulas (11).

Rheological parameters of the slurry, such as yield strength, plastic viscosity, and shear rate, have been determined experimentally in the studied temperature range 80 ÷ 40 °C in the production conditions of ceramic products of Ceramics LLP [5]. Along with rheological properties, thermal conductivity, heat capacity, and melting heat are the main elements for calculating technical parameters and play an important role in the manufacture of products by injection casting [6]. In the scientific literature, the data on thermophysical properties of the dispersed system are limited, and they theoretically confirm that mechanical failures of the dispersed system structure do not affect thermophysical properties, i.e., the value of c_p heat capacity and λ thermal conductivity [20]. The specific heat capacity of beryllium oxide has been studied experimentally and theoretically [8,21].

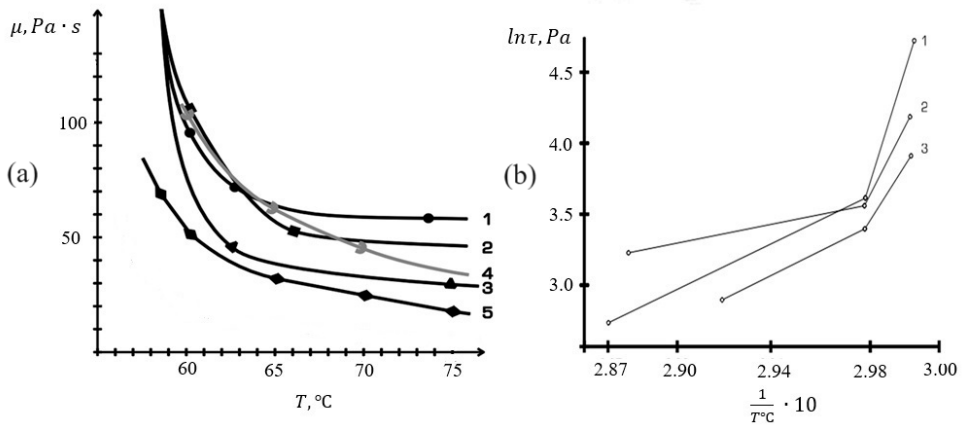

Figure 3. Experimental temperature dependences of (**a**) plastic viscosity and (**b**) shear rate during the casting process with different amounts of binder: (**a**) 1. $w = 10\%$; 2. $w = 10.7\%$; 3. $w = 11.7\%$; 4. aluminum oxide slurry Al_2O_3; 5. $w = 18\%$. (**b**) 1. $w = 11.7\%$; 2. $w = 10.7\%$; 3. $w = 10.0\%$.

In the structure of the slurry on the surface of solid particles, the adsorbed molecules of liquids significantly change some physical properties, in particular, the melting point and density increase. During melting, the solvated ligament in the slurry does not significantly change its structure. This is equivalent to the absence of latent melting heat of the solvated bond, that is, heat consumed to break the structure to change the aggregate state at the melting temperatures of the free bond.

2.2. Experimental Studies of the Casting Process

The experimental study was carried out in a ceramic casting installation developed on the basis of industrial equipment. Schematic description of the experimental ultrasonic molding unit is shown in Figure 4. Plant consists of heated tank (1), on which a two-waveguide acoustic-technological circuit (ATC) is fixed, which consists of longitudinal waveguide (2) with magnetostrictive converter (3) (MSC 15–18) and longitudinal-transverse waveguide, which is made in the form of bushing (4) with similar MSC (5) and mechanism for regulating movement of blank (6). Longitudinal waveguide (2) is introduced into working cavity of tank (1) through cover (7), on which tank fitting (8) is installed to supply compressed air to working tank [6].

The die working cavity (4) consists of a dosing chamber and a forming chamber. The die forming cavity is equipped with heating and cooling circuits. Water supplied from special thermostats is used for heating and cooling the circuits of the die and the slurry tank. To ensure the required heat removal, the possibility of controlling and regulating the temperature and flow rate of the coolant is provided. The main task is considered in this molding cavity of the die, where structure formation due to ultrasonic processing takes place.

Flow of BeO slurry considered between two concentric cylinders with the length of 108 mm, as shown in Figure 5. As BeO slurry enters the cavity between concentric cylinders, it begins to be cooled by external circulating water in three cooling zones with the lengths of $L_1 = 22$, $L_2 = 45$, and $L_3 = 41$ mm, respectively, and cooling temperature of $T_1 = 73$ °C, $T_2 = 59$ °C, and $T_3 = 45$ °C, respectively (see Figure 5b). Outer radius of inner cylinder, inner radius of outer cylinder, and outer radius of outer cylinder is $r_1 = 20$, $r_2 = 25$, and $r_3 = 26$ mm, respectively. The thickness of outer cylinders (crystallizer) wall is 1 mm. The material of inner and outer cylinders is made from steel of grade 12X18H10T. Inner radius of water circulation zones is $r_w = 36$ mm.

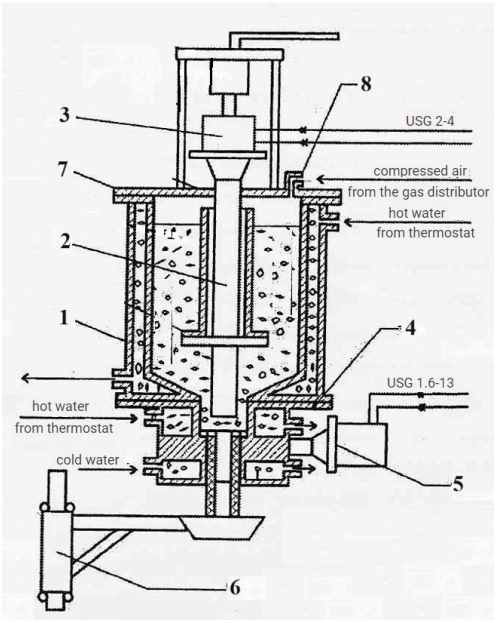

Figure 4. Diagram of industrial ultrasonic (US) molding plant: 1—heated slurry tank; 2—longitudinal waveguide; 3,5—magnetostrictive converters (MSC 15–18); 4—die (working cavity); 6—mechanism for regulating; 7—cover; 8—air supply fitting.

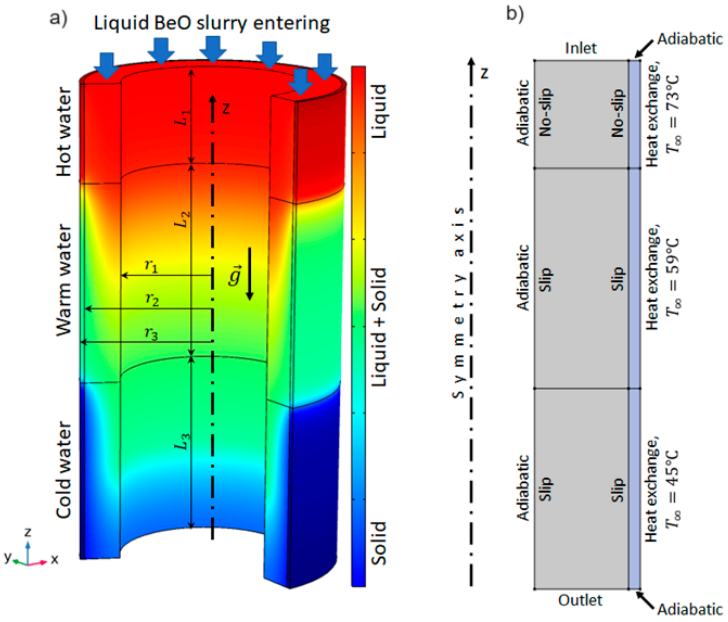

Figure 5. (**a**) 3D schematic of BeO slurry flow and solidification and (**b**) 2D domain with an imposed boundary conditions.

The slurry mass moving stationary in the annular molding cavity is cooled by water washing the tube from the outside. The molding speed is directed vertically downward along the z (Figure 5). In general, the solidification process is nonlinear, whereby as the slurry progresses and cools, the slurry changes all physical properties depending on temperature and exposure to ultrasonic forces. Thermophysical and rheological properties of the slurry are determined by the results of the experiment (Figure 3) and are expressed in the form of empirical relationships (11) [5,8].

3. Mathematical Model

The flow of BeO slurry including its solidification is described using the enthalpy–porosity approach, as proposed by Voller et al. [22], and it is a widely used technique for modeling melting and solidification [23–28]. This approach considers the damping source in the Navier–Stokes equation to force calculated velocity to equal zero when BeO slurry becomes fully solid. Damping coefficient A is introduced similarly with the permeability of porous medium, which depends on the BeO slurry liquid fraction. The model equations are derived under the following assumptions that BeO slurry flow has the following characteristics:

- Laminar due to the low casting velocity;
- Steady state;
- Weakly compressible;
- Axisymmetric.

3.1. Fluid Flow Equations

The flow of the BeO slurry is described using unsteady Navier–Stokes equations [29]

$$\rho(\vec{u}\cdot\nabla)u = -\nabla p + \nabla\cdot[\mu_{app}(\nabla\vec{u} + (\nabla\vec{u})^T)] + \rho\vec{g} - A(\vec{u} - \vec{u}_{cast}) \quad (1)$$

$$\nabla\cdot(\rho\vec{u}) = 0 \quad (2)$$

where $\vec{u}$ is the BeO slurry velocity $(\mathrm{m/s})$, ρ is the BeO slurry density $(\mathrm{kg/m^3})$, p is the pressure (Pa), μ_{app} is the apparent dynamic viscosity $(\mathrm{Pa{\cdot}s})$, and $\vec{u}_{cast} = (0, u_{cast})$ is the casting velocity.

The last term in the momentum conservation equation is utilized to account for resistance force from a solid phase with a resistance coefficient A, which is the function of liquid fraction α. It imitates the permeability of liquid–solid porous medium with the porosity of α under the enthalpy–porosity model and defined as [30,31]

$$A = C_m\frac{(1-\alpha)^2}{\alpha^3+\varepsilon} \quad (3)$$

where C_m is the mushy zone constant and has a large value as $5{\cdot}10^5\mathrm{kg/(m^3{\cdot}s)}$, and $\varepsilon = 10^{-3}$ is a small parameter that helps to avoid division by zero when α approaches zero. In pure liquid zone ($\alpha = 1$), coefficient A is zero, and it increases in the mushy zone ($0 < \alpha < 1$) from a small value to a large value $A \approx C_m/\varepsilon$, which leads to the domination of resistance force.

The liquid/solid interface is explicitly tracked, and liquid fraction α is calculated using the following expression [32].

$$\alpha = \begin{cases} 0 & if\ T < T_s \\ \frac{T-T_s}{T_l-T_s} & if\ T_s \le T \le T_l \\ 1 & if\ T > T_l \end{cases} \quad (4)$$

3.2. Energy Equation for BeO Slurry

The distribution of temperature within the BeO flow domain is obtained using the advection–conduction energy equation

$$\rho C_{p,app}\vec{u}\cdot\nabla T = \nabla\cdot(\lambda\nabla T) \quad (5)$$

where $C_{p,app} = C_p + L_H D(T)$ is the apparent specific heat capacity $(\mathrm{J/(kg{\cdot}K)})$, C_p and $L_H = 7800\ \mathrm{J/kg}$ are specific heat capacity $(\mathrm{J/(kg{\cdot}K)})$ and latent heat of solidification,

respectively, T is temperature (K), and λ is thermal conductivity $(\mathrm{W/(m{\cdot}K)})$, and function $D(T)$, which describes latent heat absorption during BeO solidification, is expressed as [33–35]

$$D(T) = \frac{2}{\Delta T\sqrt{\pi}} e^{-\left(\frac{2(T-T_m)}{\Delta T}\right)^2} \tag{6}$$

where $\Delta T = T_l - T_s = 2\ (K)$ denotes the transition zone temperature range (K), $T_m = 59$ °C is the crystallization temperature (K), and $T_l = T_m + \Delta T$ and $T_s = T_m - \Delta T$ are the liquidus and solidus temperatures (K), respectively.

3.3. Energy Equation for the Crystallizer

The distribution of temperature within the crystallizer is described using the pure conduction energy equation

$$\rho_s C_{p,s} \frac{\partial T_s}{\partial t} = \nabla{\cdot}(\lambda_s \nabla T_s) \tag{7}$$

where $\rho_s = 7900\ \mathrm{kg/m^3}$, $C_{p,s} = 500\ \mathrm{J/(kg{\cdot}K)}$, and $k_s = 15\ \mathrm{W/(m{\cdot}K)}$ denote, respectively, the density, specific heat capacity, and thermal conductivity of steel with grade 12X18H10T, and T_s is the crystallizer temperature (K).

3.4. Bingham–Papanastasiou Model

Beryllium oxide thermoplastic slurry is a non-Newtonian fluid. In addition, BeO slurry behaves differently as solidification progresses, so the yield stress is the function of temperature. According to the experimental data, the increase in the flowability of the slurry is achieved by decreasing the viscosity of the slurry with the duration of ultrasonic treatment [5,8]. As a result, as the shear stress τ increases, and part of the bound dispersion medium is released from the solvate shells, leading to an increase in the flowability of the slurry. The Shvedov–Bingham model describes the viscoplastic flow of the slurry in a limited shear rate region with an acceptable accuracy. In this study, the Bingham–Papanastasiou model is used as a regularization of the conventional Bingham model in order to overcome numerical issues within low shear rates [36,37].

The Bingham–Papanastasiou model is a modification of the plastic Bingham model, which allows the exhibition of infinitely high viscosity within low shear rates. By using a regularization parameter, this approximation could be made more accurate even at vanishingly small shear rates. The article presents flow curves of viscoplastic slurry for different values of the regularization parameter m (Figure 6). These results confirm that the Bingham–Papanastasiou model turns into the traditional Bingham model when the regularization parameter m approaches infinity [30]. According to this model, apparent viscosity is calculated as following

$$\mu_{app} = \mu_p + \frac{\tau_y}{\dot{\gamma}}\left[1 - e^{-m\dot{\gamma}}\right] \tag{8}$$

$$\dot{\gamma} = \sqrt{2S:S},\ \ S = \frac{1}{2}(\nabla\vec{u} + (\nabla\vec{u})^T) \tag{9}$$

where $\mu_p(T)$ is the plastic viscosity (Pa·s), $\tau_y(T)$ is the yield stress (Pa), $\dot{\gamma}$ is the shear rate $(\mathrm{s^{-1}})$, m is the regularization parameter (s), and S denotes strain tensor. The Bingham–Papanastasiou model reduces to the ideal Newtonian fluid model at $m \to 0$ and becomes a pure Bingham model for large values of m. In this paper, the value of $m = 50$ s was used, which shows the best approximation of the Bingham model with the Bingham–Papanastasiou regularization model.

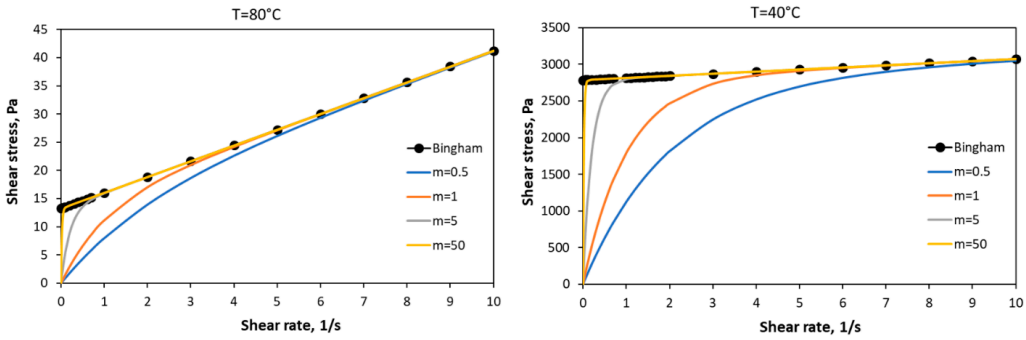

Figure 6. Bingham–Papanastasiou model for different values of regularization parameter m.

3.5. Boundary Conditions

Hot BeO slurry enters the cavity between two concentric cylinders (gray domain in Figure 5b) at a constant casting velocity u_{cast} and temperature $T_{cast} = 75$ °C. The surface of the mandrel is assumed to be adiabatic and partly no-slurry (Figure 5a,b). BeO slurry leaves the cavity with uniform outlet pressure and zero gradient of temperature. On the inner surface of the crystallizer, there is a conjugate condition between the energy equations for the BeO slurry and crystallizer. On this surface, no-slurry and slurry conditions are applied to the momentum conservation equation. The slurry condition allows the movement of the thermoplastic slurry near the wall when it starts to be cooled. The COMSOL Multiphysics software package automatically calculates the slurry velocity based on the yield stress value and velocity profile at the wall. Convective heat transfer occurs between the outer surface of the crystallizer and the cooling water. An adiabatic boundary condition is imposed to the energy equation for the crystallizer at the top and bottom surfaces of the crystallizer.

Convective heat transfer coefficient h_i, on each part of outer boundary with height L_i, is calculated from the Nusselt number using Churchill and Bernstein correlation for the external forced convection, which is valid for $RePr \gtrsim 0.2$ [36]

$$Nu = \frac{2r_3 h}{\lambda_w} = 0.3 + \frac{0.62 Re^{1/2} Pr^{1/3}}{\left[1 + \left(\frac{0.4}{Pr}\right)^{2/3}\right]^{1/4}} \left[1 + \left(\frac{Re}{282000}\right)^{5/8}\right]^{4/5} \quad (10)$$

where $Re = \frac{2r_3 Q_w}{\nu_w (r_w - r_3) L}$ and $Pr = \frac{\mu_w c_{p,w}}{\lambda_w}$ are Reynolds and Prandtl numbers, respectively, r_w is the inner radius of cooling zone, Q_w is the flow rate of circulating water in the cooling zone, and μ_w, $c_{p,w}$, and λ_w are the dynamic viscosity (Pa·s), specific heat capacity (J/(kg·K)), and thermal conductivity (W/(m·K)) of the circulating water.

4. Numerical Simulation Procedure and Model Validation

Equations (1), (2), (4) and (7) have been solved by a fully coupled finite element method using commercial software package COMSOL Multiphysics version 5.6 along with the previously stated initial and boundary conditions. An automatic Newton solver with the minimum damping factor of 10^{-4} is used to linearize the coupled nonlinear equations, and the PARDISO direct solver has been used for the solution of linear equations system. The maximum number of Newton iterations is set to 400, and the relative tolerance has been chosen as 0.001. A mapped quadrilateral mesh is used, and grid independence tests have been conducted with the calculation of the liquid fraction of BeO. It has been shown that the mesh with 10,773 total elements was enough for the analysis, and after that, the change in the calculated liquid fraction is negligible. For the discretization of fluid flow equations, second-order elements for the velocity components and linear elements for the pressure field (P2 + P1) were chosen, and quadratic Lagrange elements were chosen for the discretization of energy equations. Thermophysical and rheology properties of BeO slurry are temperature-dependent functions, and they were incorporated into the COM-

SOL Multiphysics software package using user-defined functions (UDFs). The auxiliary relations (4) and (6) are also realized using UDFs. Specified combinations of sweep type are used to extend the studies of change effect parameters.

Thermophysical and rheology properties of BeO slurry are the functions of temperature and given by the following expressions

$$\begin{aligned} \rho &= \frac{\rho_{BeO}\rho_{Bin}}{\omega\rho_{BeO}+(1-\omega)\rho_{Bin}} \\ \lambda &= 1.6 + 4.8e^{-0.017(T-273.15)} \\ C_p &= 70 + 1070e^{0.0027(T-273.15)} \\ \mu_p &= 34.955 + 3.44{\cdot}10^{14}e^{-0.494(T-273.15)} \\ \tau_y &= 18.12 + 2.121{\cdot}10^{11}e^{-0.368(T-273.15)} \end{aligned} \tag{11}$$

where the binder density is calculated by $\rho_{Bin} = 852 + 72.5cos(0.05612T - 16.7361)$ kg/m^3, $\omega = 11.7\%$ is the fraction of binder, and $\rho_{BeO} = 3020$ kg/m^3 denotes the BeO powder density.

4.1. Rheology Model Validation

Graphical illustrations of thermoplastic BeO slurry flow curves for various values of regularization parameter m in the Bingham–Papanastasiou model are given in Figure 6. It can be noted that with a high value of m, the Bingham–Papanastasiou model is a qualitative approximation to the conventional Bingham model, and with a low m to the Newtonian fluid [35]. If the shear stress is greater than the yield stress, then the rest state and yield zone for non-Newtonian fluids can be determined by numerical modeling. As can be seen from Figure 6, flow curves have different yield points at $T = 80$ °C and $T = 40$ °C, respectively. The use of the regularization parameter made it possible to approximate the BeO slurry behavior at all shear rates. That is why a more appropriate value (m = 50 s) of this parameter is selected on the base of relatively faster convergence to the solution and visual coincidence of the flow curve obtained by the Bingham–Papanastasiou model with the flow curve obtained by the conventional Bingham model for both 80 and 40 °C.

The following graphs show that the approximation can be made more and more accurate even at vanishingly low shear rates. It can be seen from Figure 6 that the value of $m = 50$ s shows best approximation of the Bingham model with the Bingham–Papanastasiou regularization model.

The evolution of velocity for different values of m along the main flow direction for 28 mm dual-zone cylindrical cavity shown in Figure 7. It shows that the BeO slurry behaves as a non-Newtonian liquid at $m = 50$ even within the hot zone of the forming cavity. As the parameter increases—$m = 0.5; 1; 5; 50$—the velocity profile varies from a parabolic profile flat plateau arising in the central zone of the channel, which is a non-deformed material. At $z = 6$ (in the hot zone), the slurry flow is fully developed, in which the slurry is practically not cooled, and the speed has a parabolic profile (Figure 7a). At $z = 0$ in the transition zone from the hot circuit to the cold circuit, the velocity profile is deformed due to a large temperature difference (Figure 7b); at $z = -8$ in the cold circuit (Figure 7c) and $z = -12$ mm at the outlet (Figure 7d), it is gradually smoothed out and the sliding effect on the side of the wall has a strong effect on the velocity profiles of the cold circuit. From the analysis of graphical dependencies, it can be seen that the smaller the value of parameter m, the greater the unevenness of the slurry flow rate, which decrease as it cools.

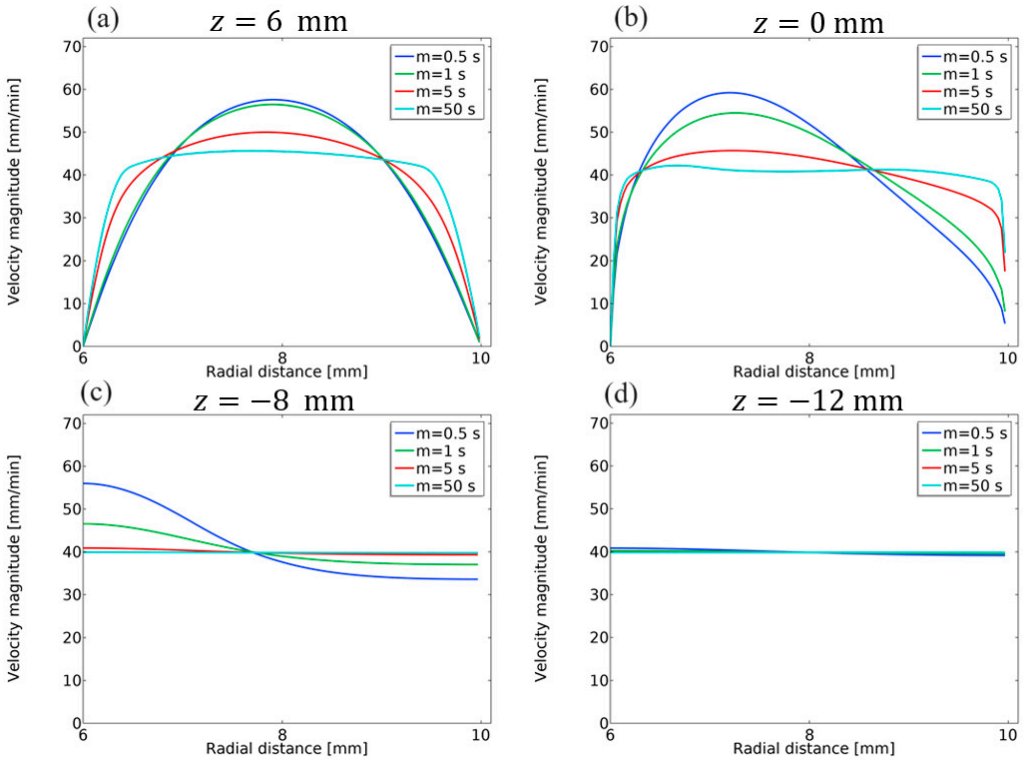

Figure 7. Evolution of velocity profile at different positions along the length of the channel (**a**) $z = 6$ mm, (**b**) $z = 0$ mm, (**c**) $z = -8$ mm, and (**d**) $z = -12$ mm for $u_{cast} = 40$ mm/min and different values of m.

4.2. CFD Model Validation

The built CFD model has been validated with the experimental data on solidification of the BeO thermoplastic slurry in the dual-zone cylinder [5]. The total height of the forming cylinder is 28 mm, the height of the hot zone is 8 mm, and the height of the cold zone 20 mm. The outer and inner diameters are 20 mm and 12 mm, respectively. The liquid BeO slurry enters the forming cylinder at a temperature $T = 80$ °C, and casting velocity $u_{cast} = 20;\ 40;\ 60;\ 80;100$ mm/min from the top of forming cylinder. The temperature of water in the hot and cold zones is 80 and 20 °C, respectively (Figure 8).

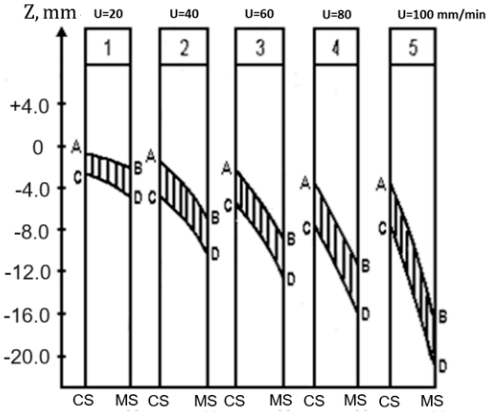

Figure 8. Position of the solidification zone depending on casting speed: AB—isotherm of "liquidus" (54 °C); CD—isotherm of "solidus" (40 °C); CS—crystallizer surface; MS—mandrel surface.

The conical input of the bushing is connected with the working tank of casting installation where the BeO slurry is kept. The slurry flows from the tank to the conical inlet of the annular cavity with an initial temperature of $t_0 = 80$ °C [5].

Figure 8 shows positions of solidification zones depending on the molding speed. Isotherm of the AB solidus corresponds to the temperature 54 °C and isotherm of the CD solidus to 40 °C.

Numerical simulations using the CFD model are conducted for different casting velocities. Figure 9 depicts the distribution of liquidus (A–B) and solidus (C–D) for different casting velocities. It is noteworthy that symbols and solid lines are correspond to the experimental and simulated data. According to the experimental data, the values of liquidus and solidus are $T = 59$ and $T = 45$ °C, respectively. As can be seen from Figure 9, there is good agreement between the simulated and experimental results, which indicates that the above-provided CFD model is capable of simulating the solidification of thermoplastic BeO slurry.

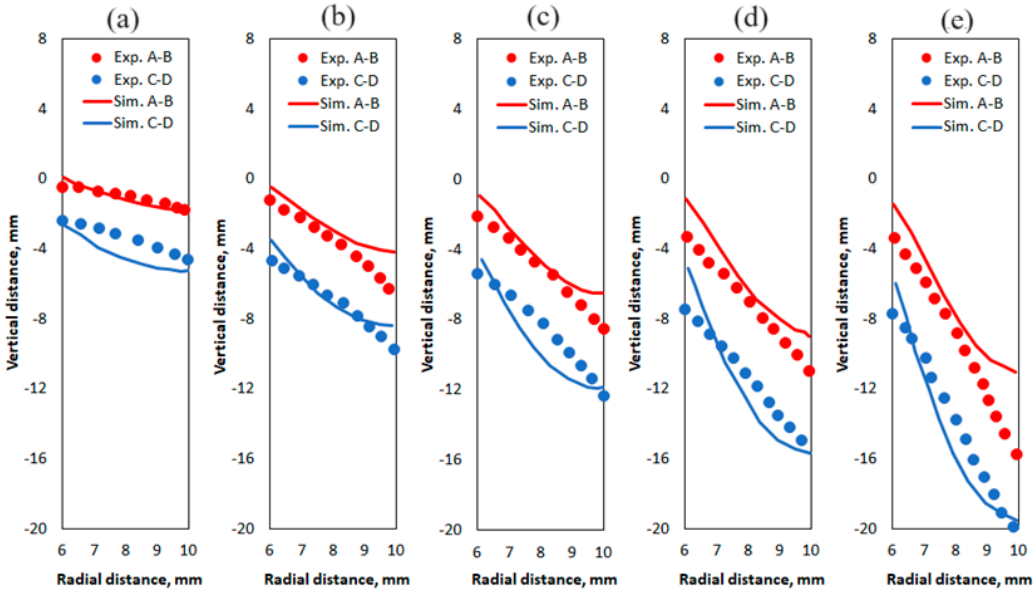

Figure 9. Simulated (solid lines) and experimental (symbols) liquidus (A–B) and solidus (C–D) for casting velocity of (**a**) 20, (**b**) 40, (**c**) 60, (**d**) 80, and (**e**) 100 mm/min.

5. Discussion of Calculated Data

5.1. The Effect of Casting Velocity

The evaluation of the effect of cooling conditions on the solidification process of beryllium ceramics is achieved by a detailed study of the profiles of casting speed, shear rate, and temperature along the concentric cylinder. The evolution of transient temperature circuits at different casting speeds (Figures 10 and 11) is presented. It can be seen from the graphs that as the casting speed increases, the solidification front becomes steeper starting from $u = 70$ mm/min. Zones of liquid, viscoplastic, and hard plastic slurry are represented by red, green, and blue colors, and it can be seen that the area of red color increases in proportion to the increase in casting speed. The reason for this phenomenon is that with an increase in the casting speed, more slurry mass enters the annular cavity, which, in turn, increases the flow of thermal convection. Another reason for such phenomena is that as the casting speed increases, the residence time of the liquid slurry decreases and the heat generated also decreases. In all the figures below, the parabolic liquidus isotherm changes to an almost horizontal front in the central zone of the cavity. In this part, a conductive heat transfer mode is preferably applied, which in turn leads to an increase in the horizontal length of the solidus isotherm. In the phase transition interval, the process proceeds at negligible speeds. According to the phase rule and experimental data, the casting system, i.e., the solid and liquid phases, are in equilibrium at a temperature of $T = 59$ °C, the zone of which is represented by a bright blue region.

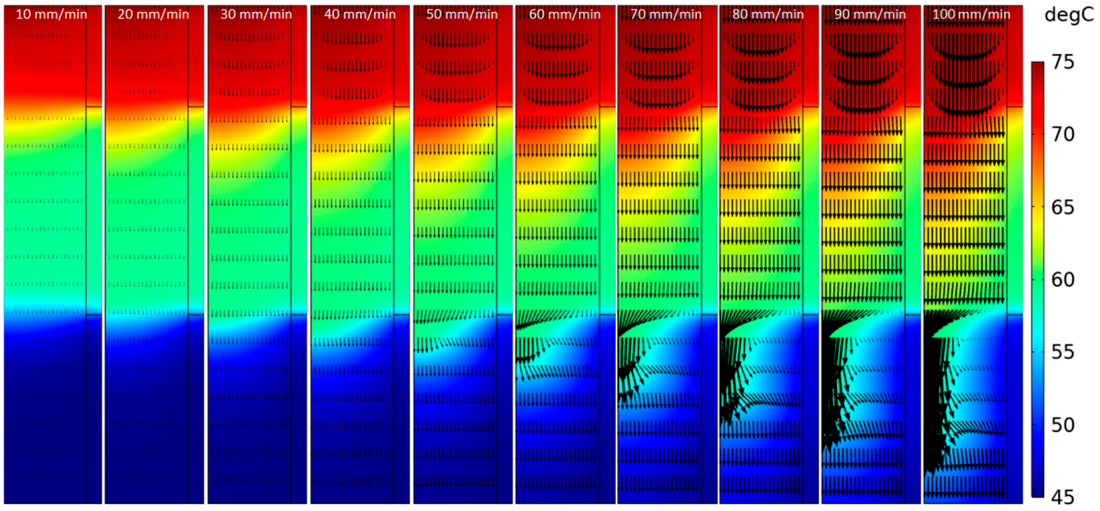

Figure 10. Temperature of BeO slurry and crystallizer for $D_2/D_1 = 1.25$ and different casting velocity.

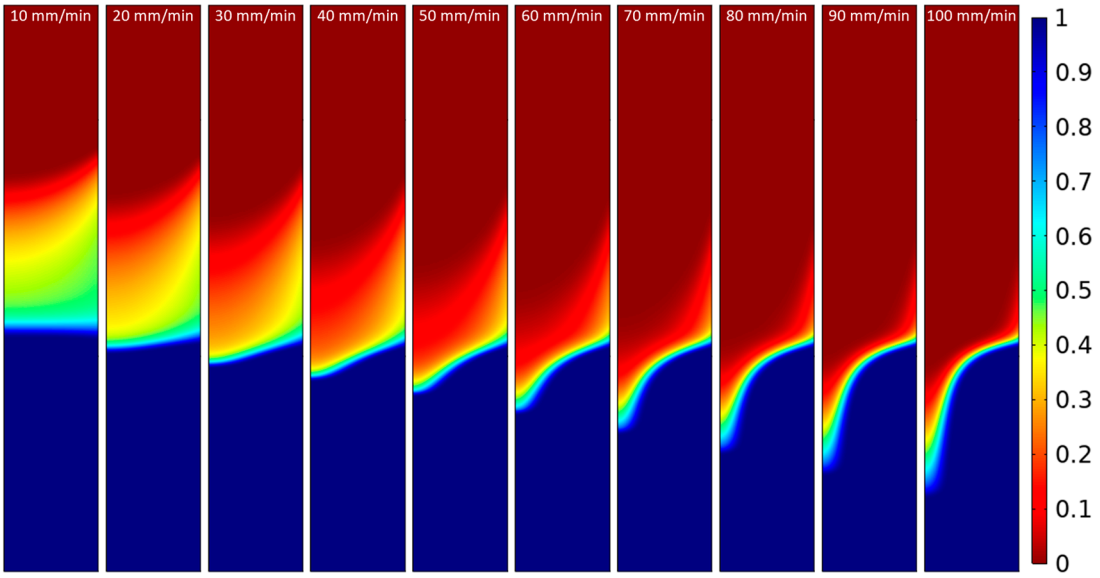

Figure 11. Solid fraction of BeO slurry for $D_2/D_1 = 1.25$ and different casting velocity.

At the end of the heat circuit, it is observed that the sliding effect has a strong effect on the cold circuit velocity profiles. The change in velocity direction in the transition from the warm loop (green) to the cold loop (blue) is due to the viscous friction force associated with an increase in casting velocity from $u = 40$ mm/min to $u = 100$ mm/min, resulting in uneven cooling and zonal liquation.

Thus, achieving a homogeneous microstructure depends on the casting speed, the temperature of warm and cold water during molding. To avoid the appearance of shrinkage defects, it is necessary to achieve the consistent development of slurry crystallization in compliance with the principle of directional solidification.

Changes in the regions of the liquid and solid zones with increasing velocity show that the depth of the viscoplastic zone of the core is stretched, forming a curved contour upon contact with the cooling wall. This is because the viscosity–temperature relationship is exponential and the deformation of the velocity profiles is determined by the magnitude of its cross-sectional variation. In the cold zone, a smaller change in the average mass temperature contributes to a decrease in the heat exchange intensity.

Figure 12 shows changes in heat flux on the inner (discontinuous lines) and outer (solid lines) walls of the mold along the length of the annular cavity at $D_2/D_1 = 1.25$ and

at different casting speeds. Obviously, the heat flux does not change significantly along the length of the hot circuit. This is due to the fact that the temperature of the coolant $T_0 = 73$ °C is practically equal to the initial temperature of the slurry, i.e., $T_0 = 75$ °C. At a distance of $z = 22$ mm, the warm circuit begins, the coolant temperature will become $T_0 = 59$ °C and the heat exchange on the inner wall will sharply increase in the following sequence: $q_{u=10} = 5089$; $q_{u=30} = 8832$; $q_{u=50} = 11.458$; $q_{u=70} = 13.368$; $q_{u=100} = 15.525$ W/m^2. The temperature gradient, having reached a maximum, begins to decline sharply due to the alignment of the temperature diagram near the wall. At a distance of $z = 67$ mm, a cold circuit is marked, where the coolant temperature is $T_0 = 45$ °C. It can be seen that the heat exchange between the slurry and the inner wall at casting rates of $u = 10$ to 30 mm/min advantageously reduces the slurry temperatures to the slurry hardening temperature.

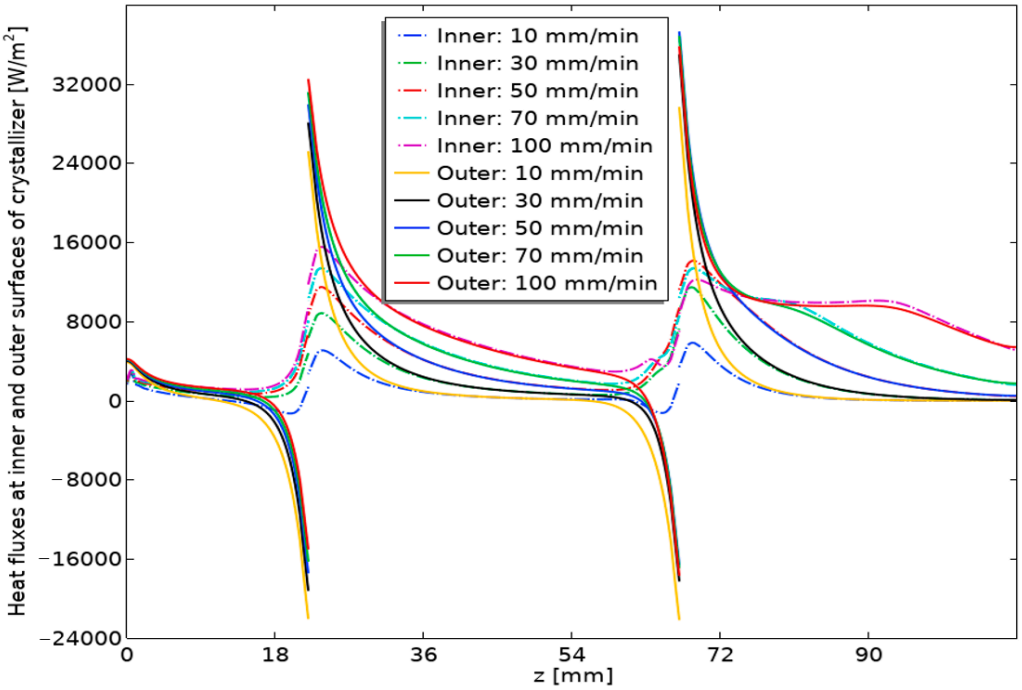

Figure 12. Change in heat flow on the inner (dashed lines) and outer (solid lines) walls of the cavity along its length for $D_2/D_1 = 1.25$ and different casting velocity.

The hot slurry transfers its heat to the inner wall of the spinneret due to internal convection, and then it is transmitted to the outer wall due to conductive thermal conductivity, only then entering the cooling water, where the heat flux vectors are directed in opposite directions. The solidification dynamics of the thermoplastic slurry as a function of the casting speed shows when the casting speed is lower than $u = 30$ mm/min, the temperature head gradient effectively influences the heat transfer coefficient like the effect of the flow rate gradient on the sliding coefficient. The intensity of free convection arising from the presence of a temperature gradient in the flow leads to a significant increase in the heat transfer of the non-isothermal surface, that is, from the slurry to the coolant.

The solidification process of the slurry mass can be estimated by changing its density along the length of the concentric channel (Figure 13). In the hot circuit, the density of the slurry practically does not change, and in the warm and cold circuit zone, it increases to 2.35 g/cm^3.

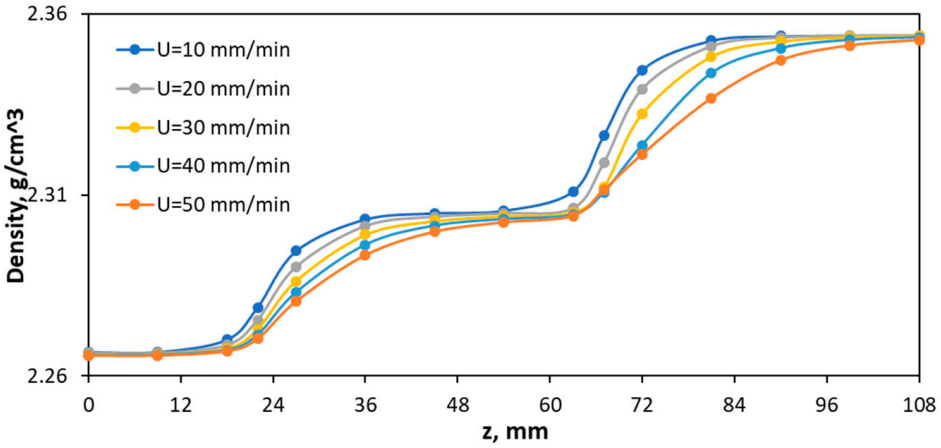

Figure 13. Averaged by cross-section BeO slurry density vs. the length of domain for $D_2/D_1 = 1.25$ and different casting velocity.

In order to optimize the solidification process, calculations are given below to evaluate the effect of casting parameters such as changes in solid state and temperature according to the casting speed over three contours and the dimensions of the D_2/D_1 cavity. A high degree of hardening of the thermoplastic slurry and uniform temperature cooling are achieved for $D_2/D_1 = 1.25$ (Figures 14 and 15). With increasing channel diameters $D_2/D_1 = 1.4$ and $D_2/D_1 = 1.5$, the degree of solidification according to the casting speed along the length of the hot zone shows a curvilinear character with a decrease in the volume fraction of the solid phase due to a significant dependence on speed and temperature. Increasing the diameters of channels $\frac{D_2}{D_1} = 1.4$ and $\frac{D_2}{D_1} = 1.5$ possibly leads to an increase in the unevenness of temperature distribution due to a decrease in pressure drop, which is explained in Figures 14 and 15. When the diameters of the annular gap increase, the mass flow rate and the value of heat content of the hot slurry increase, which leads to the slowing down of the cooling process.

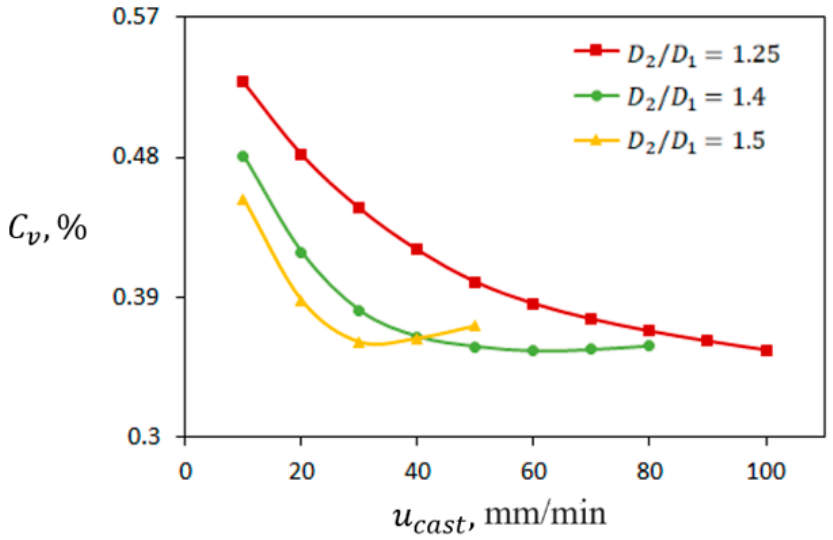

Figure 14. Volume-averaged solid fraction of BeO slurry vs. casting velocity for different D_2/D_1.

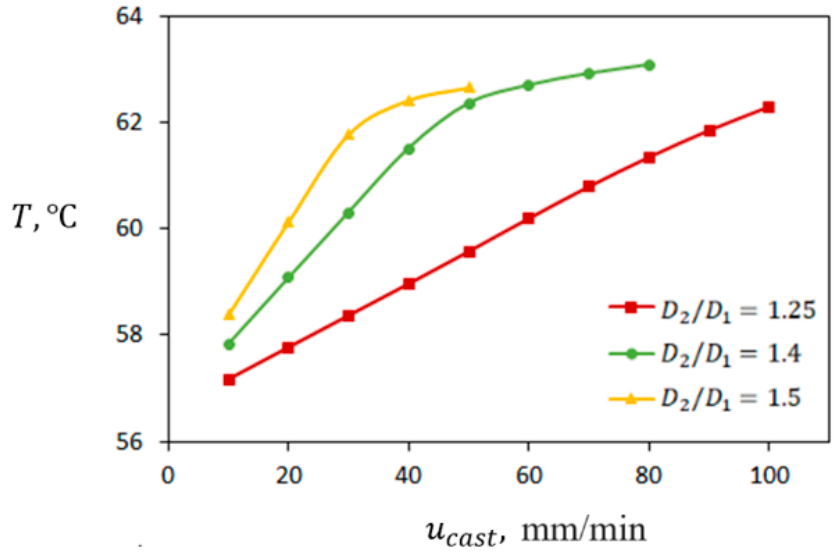

Figure 15. Volume-averaged BeO slurry temperature vs. casting velocity for different D_2/D_1 values.

5.2. The Effect of Temperature of Warm Water

Shown below are the effects of the cooling water temperature of the warm circuit of the three-contour concentric cylinder in question on the degree of solidification and on the change in slurry temperature as the cylinder diameters increase (Figures 16 and 17). It can be seen that in the warm circuit, increasing the diameter of the channel has little effect on the degree of solidification, confirming the dimensional effect. In this case, in the temperature range from 59 to 55, a sharper bend is observed at $D_2/D_1 = 1.25$, which reaches the limit value of the hardness state. The relative change in the degree of solidification, considering the temperature of the phase transition in the warm circuit established by the test method, is $35 - 0.79$.

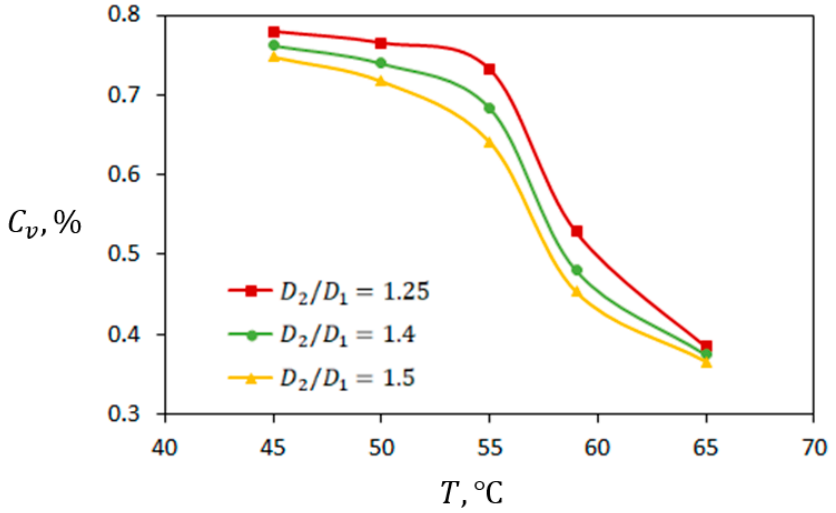

Figure 16. Volume-averaged solid fraction of BeO slurry vs. temperature of warm water for different D_2/D_1 values.

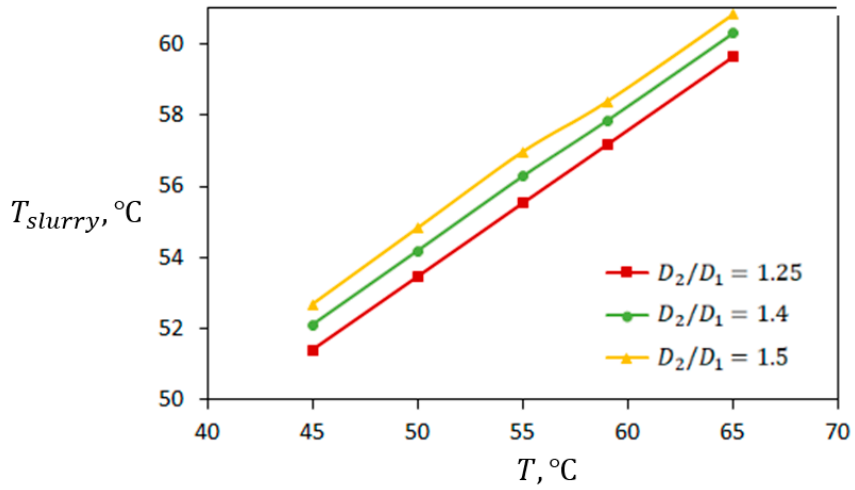

Figure 17. Volume-averaged BeO slurry temperature vs. temperature of warm water for different D_2/D_1 values.

5.3. The Effect of Temperature of Cold Water

The effect of the cooling water temperature of the cold circuit on the degree of solidification and on the change in the temperature demonstrates a smooth crystallization rate at different cylinder diameters (Figures 18 and 19). It is noticeable that a high proportion of the solid phase formed is achieved at $D_2/D_1 = 1.25$, which has a significant effect on the final casting structure and its properties.

The presented effects of the casting parameters are as follows: the casting speed of the hot circuit on the degrees of solid phase and on the temperature of the slurry, the temperature of the warm and cold circuits on the degrees of solid phase, and the temperature of the slurry make it possible to predict thermal and shrinkage processes during the gradual replacement of the liquid with solid phases.

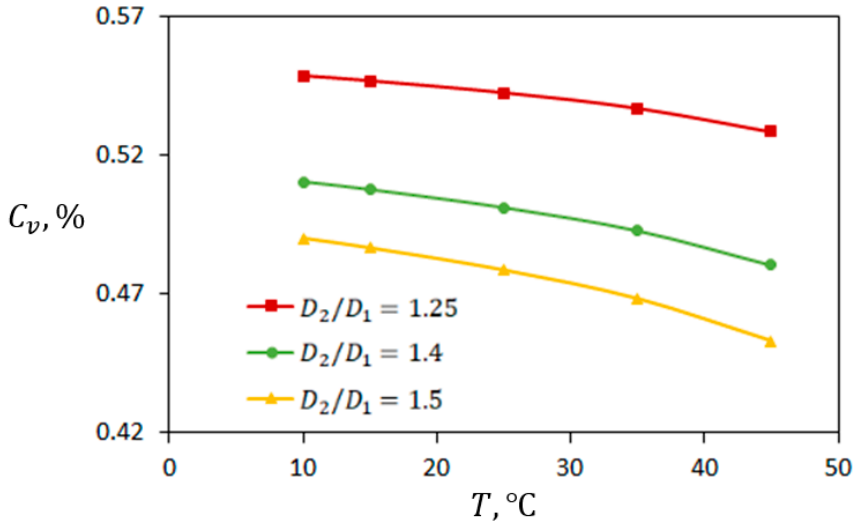

Figure 18. Volume-averaged solid fraction of BeO slurry vs. temperature of cold water for different D_2/D_1 values.

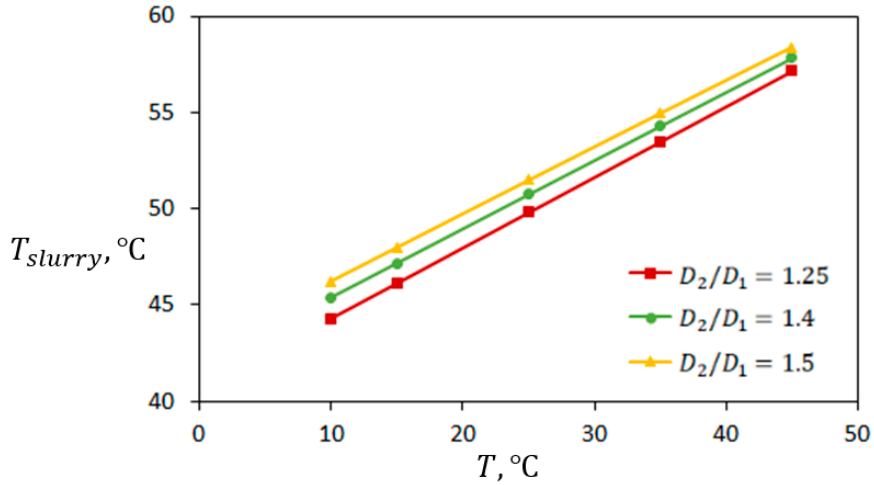

Figure 19. Volume-averaged BeO slurry temperature vs. temperature of cold water for different D_2/D_1 values.

6. Conclusions

The modeling of the solidification process of beryllium oxide slurry with regard to phase transitions and the optimization of casting technology have been performed using the COMSOL Multiphysics software package. The evaluation of the effect of cooling conditions on the solidification process of beryllium ceramics is achieved by a detailed study of the profiles of casting speed, shear rate, and temperature along the concentric cylinder. Based on the results of studying the influence of the optimal control parameters of the solidification process on the homogeneity of the product, the following conclusions can be drawn:

- Experimentally determined intervals of phase transitions at different casting speeds of beryllium ceramics are compared with phase transitions obtained using the Bingham–Papanastasiou model.
- Parametric studies have been carried out on the changes in the hardening degree and the temperature of a suspension in three hot, warm, and cold circuits, depending on casting speed and cylinder dimensions.
- Casting velocities up to 30 mm/min will be optimal since further increasing their values does not change the average temperature of the BeO slurry.
- Maintaining the temperature of the warm water zone up to 55 °C is an optimal condition because its further increase leads to sharp decrease in the solid fraction after cooling.
- The solid fraction of BeO slurry is less sensitive to the temperature of cold water.

The numerical results carried out show adequate agreement with the available experimental data. The results obtained in this work and the quantitative values given for the different casting parameters can be useful in the production process when evaluating possible solidification conditions to obtain castings of higher quality.

Author Contributions: Conceptualization, Z.S. and B.A.; methodology, Z.S., T.B. and B.A.; software, B.A.; validation, B.A. and G.R.; formal analysis, T.B. and G.R.; investigation, Z.S. and T.B.; resources, G.R.; data curation, Z.S. and G.R.; writing—original draft preparation, Z.S., T.B. and B.A.; visualization, G.R. and T.B.; project administration, Z.S.; funding acquisition, Z.S. All authors have read and agreed to the published version of the manuscript.

Funding: The results of this research were funded by the Committee of Science of the Ministry of Science and Higher Education of the Republic of Kazakhstan, grant number AP19680086 for 2023–2025.

Institutional Review Board Statement: Not applicable.

Informed Consent Statement: Not applicable.

Data Availability Statement: Data are contained within the article.

Conflicts of Interest: The authors declare no conflicts of interest.

References

1. Wei, J.; Zhou, W.; Zhou, W.; Li, S.; Shen, P.; Ren, S.; Hu, A. Modified Embedded Atom Method Potential for Modeling the Thermodynamic Properties of High Thermal Conductivity Beryllium Oxide. *ACS Omega* **2019**, *4*, 6339–6346. [CrossRef] [PubMed]
2. Walsh, K.A. *Beryllium Chemistry and Processing*; ASM International: Materials Park, OH, USA, 2009. [CrossRef]
3. Kiiko, V.S.; Vaispapir, V.Y. Thermal Conductivity and Prospects for Application of BeO Ceramic in Electronics. *Glass Ceram.* **2015**, *71*, 387–391. [CrossRef]
4. Sardarian, M.; Mirzaee, O.; Habibolahzadeh, A. Mold filling simulation of low pressure injection molding (LPIM) of alumina: Effect of temperature and pressure. *Ceram. Int.* **2017**, *43*, 28–34. [CrossRef]
5. Zhapbasbayev, U.; Ramazanova, G.; Kenzhaliev, B.; Sattinova, Z.; Shakhov, S. Experimental and calculated data of the beryllium oxide slurry solidification. *Appl. Therm. Eng.* **2016**, *96*, 593–599. [CrossRef]
6. Sattinova, Z.K.; Bekenov, T.N.; Assilbekov, B.K.; Ramazanova, G.I.; Zhapbasbayev, U.K.; Nussupbek, Z.T. Mathematical modeling of the rheological behavior of thermoplastic slurry in the molding process of beryllium ceramics. *Ceram. Int.* **2022**, *48*, 31102–31110. [CrossRef]
7. Agranat, B.A.; Gudovich, A.P. *Ultrasound Powder Metallurgy*; Metallurgy: Moscow, Russia, 1986. (In Russian)
8. Shakhov, S.A.; Bitsoev, G.D. *Application of Ultrasound in the Manufacture of High Thermal Conductivity Ceramic Articles*; Ust'-Kamenogorsk, Kazakhstan, 1999. (In Russian)
9. Miyamoto, K.; Miyamoto, H.; Takahashi, Y.; Taguchi, H. Preparation of Al_2O_3 ceramics by low pressure injection molding method. *Bull. Inst. Chem. Res.* **1986**, *64*, 287–291.
10. Dobrovolsky, A.G. *Slip Casting*; Metallurgy: Moscow, Russia, 1977. (In Russian)
11. Weiß, M.; Maurath, J.; Willenbacher, N.; Koos, E. Shrinkage and dimensional accuracy of porous ceramics derived from capillary suspensions. *J. Eur. Ceram. Soc.* **2019**, *39*, 1887–1892. [CrossRef]
12. Shakhov, S.A.; Gagarin, A.E. Rheological characteristics of thermoplastic disperse systems treated with ultrasound. *Glass Ceram.* **2008**, *65*, 122–124. [CrossRef]
13. Ruan, Z.-H.; Gao, X.-Y.; Yuan, Y.; Tan, H.-P. Determining the heat transfer coefficient during the continuous casting process using stochastic particle swarm optimization. *Case Stud. Therm. Eng.* **2021**, *28*, 101439. [CrossRef]
14. Papanastasiou, T.C.; Boudouvis, A.G. Flows of viscoplastic materials: Models and computations. *Comput. Struct.* **1997**, *64*, 677–694. [CrossRef]
15. Jabbari, M.; Bulatova, R.; Tok, A.I.Y.; Bahl, C.R.H.; Mitsoulis, E.; Hattel, J.H. Ceramic tape casting: A review of current methods and trends with emphasis on rheological behaviour and flow analysis. *Mater. Sci. Eng. B* **2016**, *212*, 39–61. [CrossRef]
16. Mehmood, A.; Khan, W.A.; Mahmood, R.; Rehman, K.U. Finite Element Analysis on Bingham–Papanastasiou Viscoplastic Flow in a Channel with Circular/Square Obstacles: A Comparative Benchmarking. *Processes* **2020**, *8*, 779. [CrossRef]
17. Kiiko, V.S.; Vaispapir, V.Y. The fabrication technological abilities and the properties of the ceramic products on base of the mixture of low- and high-fired BeO-powders. *Novye Ogneupory (New Refract.)* **2016**, *8*, 55–58. (In Russian)
18. Balkevich, V.L.; Mosin, Y.M. *Rheological Properties of Ceramic Mass*; Moscow Institute of Chemical Technology named after, D.I. Mendeleev: Moscow, Russia, 1983. (In Russian)
19. Ammosova, S.; Cano Cano, L.; Schuschnigg, S.; Kukla, C.; Mönkkönen, K.; Suvanto, M.; Gonzalez-Gutierrez, J. Effect of metal particle size and powder volume fraction on the filling performance of powder injection moulded parts with a microtextured surface. *Precis. Eng.* **2021**, *72*, 604–612. [CrossRef]
20. Dvinskikh, Y.V.; Popil'skii, R.Y.; Kostin, L.I.; Kulagin, V.V. The thermophysical properties of thermoplastic cast slips of some highly refractory oxides. *Refractories* **1979**, *20*, 1573–9139. [CrossRef]
21. Bradshaw, P.; Cebeci, T. *Physical and Computational Aspects of Convective Heat Transfer*; Springer: Berlin/Heidelberg, Germany, 1984. [CrossRef]
22. Voller, V.R.; Cross, M.; Markatos, N.C. An Entalpy Method for Convection/Diffusion Phase Change. *Int. J. Numer. Methods Eng.* **1987**, *24*, 271–284. [CrossRef]
23. Brent, A.D.; Voller, V.R.; Reid, K.J. Enthalpy-porosity technique for modeling convection-diffusion phase change: Application to the melting of a pure metal. *Numer. Heat Transf.* **1988**, *13*, 297–318. [CrossRef]
24. Viswanath, R.; Jaluria, Y. A comparison of different solution methodologies for melting and solidification problems in enclosures. *Numer. Heat Transf. Part B Fundam.* **1993**, *24*, 77–105. [CrossRef]
25. Vogel, J.; Felbinger, J.; Johnson, M. Natural convection in high temperature flat plate latent heat thermal energy storage systems. *Appl. Energy* **2016**, *184*, 184–196. [CrossRef]
26. Fadl, M.; Eames, P.C. Numerical investigation of the influence of mushy zone parameter Amush on heat transfer characteristics in vertically and horizontally oriented thermal energy storage systems. *Appl. Therm. Eng.* **2019**, *151*, 90–99. [CrossRef]
27. Chakraborty, P.R. Enthalpy porosity model for melting and solidification of pure-substances with large difference in phase specific heats. *Int. Commun. Heat Mass Transf.* **2017**, *81*, 183–189. [CrossRef]

28. Yamamoto, T.S.; Komarov, V. Influence of ultrasound irradiation on transient solidification characteristics in DC casting process: Numerical simulation and experimental verification. *J. Mater. Process. Technol.* **2021**, *294*, 117116. [CrossRef]
29. Mehalaine, K.; Lafri, D. Improving the energy release of a latent heat storage with multiple phase change materials loading and partition shaping. *Appl. Therm. Eng.* **2023**, *230*, 120679. [CrossRef]
30. Rubinetti, D.; Weiss, D.A.; Chaudhuri, A.; Kraniotis, D. Convective Melting Modeling Approach for Phase Change Materials with Variable Boundary Heating. In Proceedings of the 59th Conference on Simulation and Modelling, Oslo Metropolitan University, Oslo, Norway, 26–28 September 2018; Linköping Electronic Conference Proceedings. Volume 153, pp. 103–110. [CrossRef]
31. Atal, A.; Wang, Y.; Harsha, M.; Sengupta, S. Effect of porosity of conducting matrix on a phase change energy storage device. *Int. J. Heat Mass Transf.* **2016**, *93*, 9–16. [CrossRef]
32. Mohamed Moussa, E.I.; Karkri, M. A numerical investigation of the effects of metal foam characteristics and heating/cooling conditions on the phase change kinetic of phase change materials embedded in metal foam. *J. Energy Storage* **2019**, *26*, 100985. [CrossRef]
33. Soto, H.P.; Martins-Costa, M.L.; Fonseca, C.; Frey, S. A numerical investigation of inertia flows of Bingham-Papanastasiou fluids by an extra stress-pressure-velocity galerkin least-squares method. *J. Braz. Soc. Mech. Sci. Eng.* **2010**, *32*, 450–460. [CrossRef]
34. Lampaert, S.G.E.; van Ostayen, R.A.J. Experimental results on a hydrostatic bearing lubricated with a magnetorheological fluid. *Curr. Appl. Phys.* **2019**, *19*, 1441–1448. [CrossRef]
35. Jeong, J.; Chuta, E.; Ramézani, H.; Guillot, S. Rheological properties for fresh cement paste from colloidal suspension to the three-element Kelvin–Voigt model. *Rheol. Acta* **2020**, *59*, 47–61. [CrossRef]
36. Bergman, T.L.; Lavine, A.S.; Incropera, F.P. *Fundamentals of Heat and Mass Transfer*; John Wiley & Sons: Hoboken, NJ, USA, 2011.
37. Memon, A.A.; Memon, M.A.; Bhatti, K.; Khan, I.; Alshammari, N.; Al-Johani, A.S.; Hamadneh, N.N.; Andualem, M. Thermal decomposition of propylene oxide with different activation energy and Reynolds number in a multicomponent tubular reactor containing a cooling jacket. *Sci. Rep.* **2022**, *12*, 4169. [CrossRef] [PubMed]